This is a repository copy of *Echo planar imaging–induced errors in intracardiac 4D flow MRI quantification*.

White Rose Research Online URL for this paper:
https://eprints.whiterose.ac.uk/181554/

Version: Published Version

# Echo planar imaging–induced errors in intracardiac 4D flow MRI quantification

**Jos J. M. Westenberg**[1] | **Hans C. van Assen**[1] | **Pieter J. van den Boogaard**[1] |
**Jelle J. Goeman**[2] | **Hicham Saaid**[3] | **Jason Voorneveld**[4] | **Johan Bosch**[4] | **Sasa Kenjeres**[5] |
**Tom Claessens**[6] | **Pankaj Garg**[7] | **Marc Kouwenhoven**[8] | **Hildo J. Lamb**[1]

[1]CardioVascular Imaging Group, Department of Radiology, Leiden University Medical Center, Leiden, the Netherlands

[2]Department of Biomedical Data Sciences, Leiden University Medical Center, Leiden, the Netherlands

[3]Institute Biomedical Technology, Ghent University, Ghent, Belgium

[4]Department of Biomedical Engineering, Erasmus Medical Center Rotterdam, Rotterdam, the Netherlands

[5]Department of Chemical Engineering, Delft University of Technology, Delft, the Netherlands

[6]Department of Materials, Textiles and Chemical Engineering, Ghent University, Ghent, Belgium

[7]Department of Infection, Immunity and Cardiovascular Disease, University of Sheffield, Sheffield, UK

[8]Department of MR R&D-Clinical Science, Philips, Best, the Netherlands

**Correspondence**
Jos J. M. Westenberg, CardioVascular Imaging Group, Department of Radiology, Leiden University Medical Center, Albinusdreef 2, 2333 ZA Leiden, the Netherlands.
Email: j.j.m.westenberg@lumc.nl

**Funding information**
Dutch Heart Foundation; Grant No. CVON2017-08-RADAR (for H.C.v.A.)

**Purpose:** To assess errors associated with EPI-accelerated intracardiac 4D flow MRI (4DEPI) with EPI factor 5, compared with non-EPI gradient echo (4DGRE).
**Methods:** Three 3T MRI experiments were performed comparing 4DEPI to 4DGRE: steady flow through straight tubes, pulsatile flow in a left-ventricle phantom, and intracardiac flow in 10 healthy volunteers. For each experiment, 4DEPI was repeated with readout and blip phase-encoding gradient in different orientations, parallel or perpendicular to the flow direction. In vitro flow rates were compared with timed volumetric collection. In the left-ventricle phantom and in vivo, voxel-based speed and spatio-temporal median speed were compared between sequences, as well as mitral and aortic transvalvular net forward volume.
**Results:** In steady-flow phantoms, the flow rate error was largest (12%) for high velocity (>2 m/s) with 4DEPI readout gradient parallel to the flow. Voxel-based speed and median speed in the left-ventricle phantom were ≤5.5% different between sequences. In vivo, mean net forward volume inconsistency was largest (6.4 ± 8.5%) for 4DEPI with nonblip phase-encoding gradient parallel to the main flow. The difference in median speed for 4DEPI versus 4DGRE was largest (9%) when the 4DEPI readout gradient was parallel to the flow.
**Conclusions:** Velocity and flow rate are inaccurate for 4DEPI with EPI factor 5 when flow is parallel to the readout or blip phase-encoding gradient. However, mean differences in flow rate, voxel-based speed, and spatio-temporal median

speed were acceptable (≤10%) when comparing 4DEPI to 4DGRE for intracardiac flow in healthy volunteers.

**KEYWORDS**

4D flow MRI, echo planar imaging, intracardiac blood flow, phase-contrast MRI

## 1 | INTRODUCTION

Since its introduction in the 1990s,[1–3] 4D flow MRI has been recognized for its unprecedented ability for in vivo hemodynamic evaluation. However, its time-resolved multidirectional velocity encoding is associated with long scan times. To facilitate clinical translation of intracardiac 4D flow MRI, various acceleration techniques have been suggested. Sensitivity-encoding[4] acceleration has been applied to 2D flow quantification[5–7] as well as 4D flow MRI.[8,9] Echo planar imaging[10] using moderate EPI factors was applied without[11] and in combination with SENSE[12,13] for intracardiac blood flow, to enable scanning times below 10 minutes.

Echo planar imaging has several limitations associated with its use. Even for moderate EPI factors, systematic quantitative inaccuracies are introduced.[14–17] The oscillatory readout gradient creates velocity-dependent phase shifts at every odd echo.[14] Additionally, the unipolar blip phase-encoding gradient creates accumulated phase shifts due to motion, resulting in a modulated point spread function that negatively affects spatial resolution.[14] Furthermore, the prolonged readout for EPI sequences may lead to substantial ghosting artifacts[15,16] and more prominent flow displacement.[17]

Dillinger et al[18] investigated the limitations of EPI in 4D flow MRI by comparing EPI and non-EPI gradient echo (GRE) using in silico simulations and in vitro experiments for steady flow through a stenotic U-bend phantom under high-flow (2.2 m/s peak velocity) conditions. Their experiments confirmed that for flow in the readout or blip phase-encoding gradient direction, 4DEPI is inferior to non-EPI 4DGRE 4D flow MRI, with substantial errors in local peak velocities near the stenosis, flow displacement artifacts, and local loss of spatial resolution. Dillinger et al compared local velocities between different scan orientations, but did not assess the effect on flow rate. Furthermore, they performed in silico and in vitro experiments only, while in vivo intracardiac 4D flow was not evaluated, nor was the scan orientation considered with flow perpendicular to the readout and blip phase-encoding gradient.

The aim of the current study is to evaluate EPI-related errors in flow rate and velocity in in vivo intracardiac EPI versus non-EPI 4D flow MRI. This will be investigated first through in vitro experiments in straight tubes with steady flow and in a left-ventricle (LV) phantom with pulsatile flow. In both configurations, effects of the orientations of the readout and blip phase-encoding gradient with respect to the flow direction will be evaluated. Finally, the evaluation will be extended to in vivo with 4DEPI and 4DGRE acquisitions in 10 healthy volunteers.

## 2 | METHODS

Three types of experiments were performed on the same 3T MRI scanner (Ingenia; Philips Healthcare, Best, the Netherlands): (1) steady flow through straight tubes, (2) pulsatile flow in an LV phantom, and (3) whole-heart 4D flow MRI in 10 healthy volunteers. Experiment 1 was performed using scanning software release R5.6, whereas the other experiments used software release R5.3. A combination of a FlexCoverage Posterior coil in the tabletop with an anterior torso coil was used. In all experiments, two types of 4D flow MRI sequences were used: standard nonsegmented GRE (4DGRE) without EPI acceleration, and acquisitions with EPI (4DEPI5) using EPI factor 5 (i.e., five k-space lines were acquired within the same TR for every velocity encoding gradient). For experiment 1, 4DEPI3 using EPI factor 3 was also performed. The 4DEPI sequence was designed from the 4DGRE sequence but only with EPI readout added. Other scan parameters were kept identical. For both 4DGRE and 4DEPI, no fat suppression or saturation pulses were used.

With 3D acquisitions, two phase-encoding gradients (one in-plane and one in-slice direction) were applied. For EPI, a so-called blip phase-encoding gradient (usually in in-plane y-direction) and nonblip phase-encoding gradient are used. The 4DEPI was repeated with different orientations of the respective gradients with respect to the flow direction. For naming of the respective acquisitions, "ro," "bp," or "nbp" was added after 4DEPI5, in which "ro" represents the orientation with readout gradient parallel to the flow direction; "bp" represents the orientation with blip phase-encoding gradient parallel to the flow; and "nbp" represents the orientation with nonblip phase-encoding gradient parallel to the flow. The acquisition volume orientation is added to the acquisition name. This naming definition will be used for all experiments.

All 4DEPI and 4DGRE acquisitions used SENSE with factor 2. The main acquisition parameters are presented in Supporting Information Table S1A,B. The 4D flow MRI acquisitions in vivo were performed with free breathing without respiratory-motion compensation. Velocity encoding was performed using simple four-point encoding,[19] meaning a combination of a flow-compensated acquisition followed by three consecutive velocity-encoded acquisitions in the three orthogonal directions.

Experiment 1 with steady flow through straight tubes was performed to evaluate EPI-related errors associated with flow along the three respective gradient directions, as well as the influence of EPI factor, velocity encoding (Venc), and velocity magnitude (i.e., speed). Steady flow was applied through two straight tubes: one with 1.0-cm inner diameter (for a fully developed flow profile with 50 mL/s flow rate, the maximum velocity will be 127 cm/s,

but will be lower for non-fully developed flow), and one with 0.7-cm inner diameter (for fully developed flow, the expected maximum velocity is 260 cm/s). The setup is illustrated in Figure 1A. Steady flow was generated by a Sarns centrifugal pump connected to a Delphin power supply and a Sarns control module (3M Healthcare, Borken, Germany) located outside the scanner room and connected with supplying and returning tubes to the phantom. As a circulating fluid, 6 L of water was used at room temperature doped with 30 mL $T_1$-shortening gadolinium contrast (Dotarem; Guerbet, Gorinchem, the Netherlands). The contrast agent had a concentration of 0.5 mmol/mL and relaxivity of 3.4 $mmol^{-1}.L.s^{-1}$, resulting in a theoretical $T_1$ of 114 ms.[20] The tubes were submerged in a water-filled container. The set flow rate was calibrated by timed volumetric collection with beaker and stopwatch at the outlet of the returning tube.
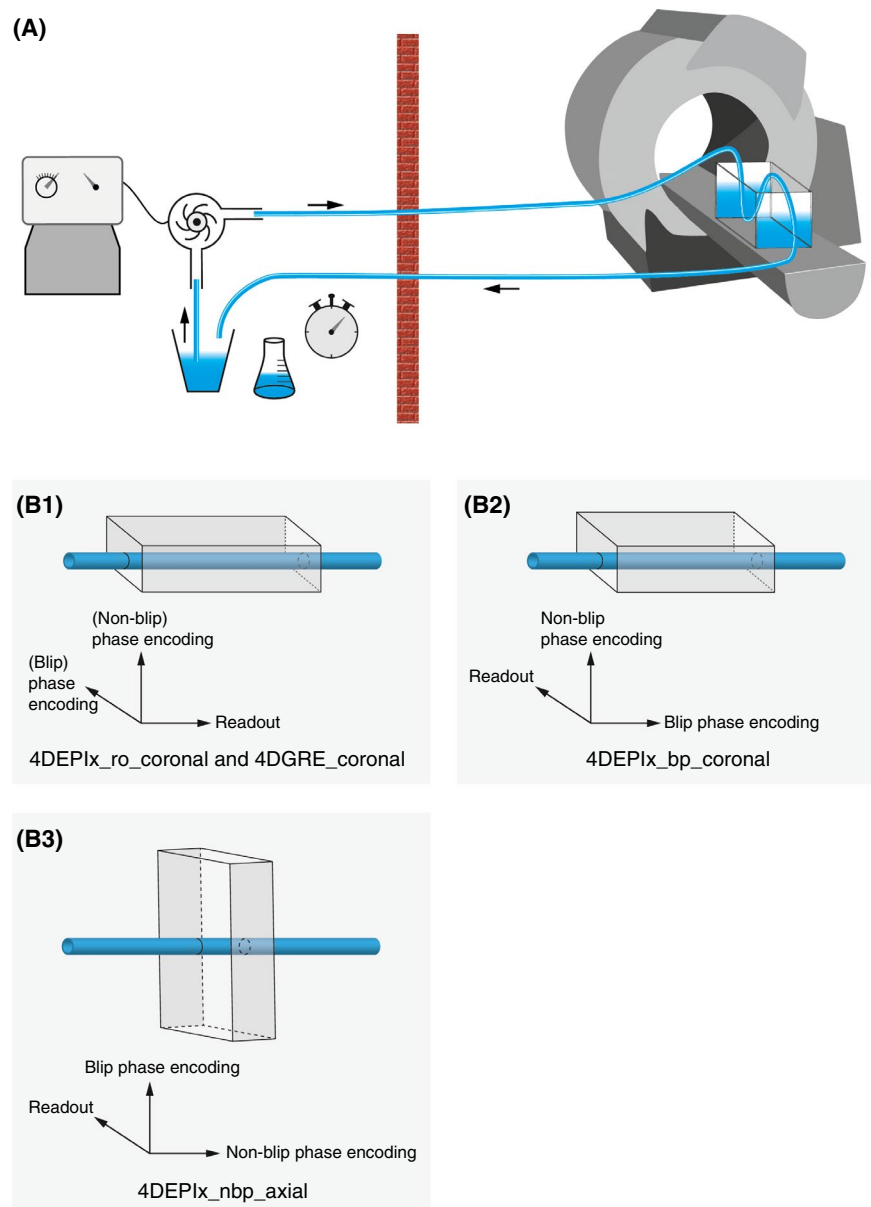


**FIGURE 1** (A) Phantom setup for experiment 1. A tank with straight tube phantom is positioned inside the MRI scanner. A pump outside the scanner room maintains steady flow, which is calibrated by timed volumetric collection at the returning tube. (B) The orientations of the 4D flow MRI acquisitions with respect to the main flow direction in the tube. In (1), 4DEPI5_ro_coronal refers to the coronally oriented EPI acquisition with the readout gradient aligned parallel to the main flow direction; in (2), 4DEPI5_bp refers to the coronally oriented EPI acquisition with the blip phase-encoding gradient aligned parallel to the main flow direction; and in (3), 4DEPI5_nbp_axial refers to the axially oriented EPI acquisition with the readout and blip phase-encoding gradient both perpendicular to the main flow direction. The 4D gradient echo (4DGRE) has the same orientation as 4DEPI5_ro_coronal. The schematically drawn scan volumes are not up to scale with the phantom dimensions

Physiology simulation was used for pseudo-electrocardiogram gating at 120 bpm. Retrospective gating with five reconstructed phases was used. The acquisition volume was planned first coronally (i.e., slices parallel to the flow) and next, axially (i.e., slices perpendicular to the flow). In coronal orientation, acquisitions were performed with the readout gradient aligned parallel to the flow (i.e., 4DEPIx_ro_coronal, where x is either EPI factor 5 or 3) and another with the blip phase-encoding gradient parallel to the flow (i.e., 4DEPIx_bp_coronal). For the axially oriented acquisition (4DEPIx_nbp_axial), both readout and blip phase-encoding gradients were perpendicular to the flow (Figure 1B, Table 1). Standard non-EPI accelerated 4DGRE was performed in the same orientation as 4DEPIx_ro_coronal.

**TABLE 1** Orientation of the MRI acquisitions for three experiments

| Acquisition | Volume orientation | Main flow direction |
|---|---|---|
| Experiment 1—straight tubes | | |
| 4DEPIx_ro_coronal | Coronal | Readout |
| 4DEPIx_bp_coronal | Coronal | Blip phase-encoding |
| 4DEPIx_nbp_axial | Axial | Nonblip phase-encoding |
| 4DGRE_coronal | Coronal | Readout |
| Experiment 2—LV phantom | | |
| 4DEPI5_ro_LA | Axial (long-axis) | Readout |
| 4DEPI5_bp_LA | Axial (long-axis) | Blip phase-encoding |
| 4DEPI5_nbp_SA | Coronal (short-axis) | Nonblip phase-encoding |
| 4DGRE_LA | Axial (long-axis) | Phase-encoding |
| Experiment 3—healthy volunteers | | |
| 4DEPI5_ro_LA | Long-axis | Readout |
| 4DEPI5_bp_LA | Long-axis | Blip phase-encoding |
| 4DEPI5_nbp_SA | Short-axis | Nonblip phase-encoding |
| 4DGRE_LA | Long-axis | Readout |

*Note:* For experiment 1, 4DEPIx_ro_coronal refers to EPI acquisition with the readout gradient aligned parallel to the main flow direction and reconstructed planes in coronal orientation; 4DEPIx_bp_coronal refers to EPI acquisition with the blip phase-encoding gradient aligned parallel to the main flow direction and reconstructed planes in coronal orientation; and 4DEPIx_nbp_axial refers to EPI acquisition with the readout and blip phase-encoding gradient both perpendicular to the main flow direction and reconstructed planes in axial orientation. The "x" after EPI is either 5 or 3, and refers to EPI factor 5 or 3. For experiments 2 and 3, 4DEPI5_ro_LA refers to EPI factor of 5 acquisition with the readout gradient aligned parallel to the main flow direction; 4DEPI5_bp_LA refers to EPI acquisition with the blip phase-encoding gradient aligned parallel to the main flow direction; and 4DEPI5_nbp_SA refers to EPI acquisition with the readout and blip phase-encoding gradient both perpendicular to the main flow direction.
Abbreviations: LA, long-axis; SA, short-axis.

The 4DEPI and 4DGRE acquisitions were repeated without flow with the pump switched off after 5 minutes of waiting time. These data were used for phase offset background correction by voxel-based velocity subtraction.[21] Image analysis was performed using *CAAS MR Solutions* 5.1 (Pie Medical Imaging, Maastricht, The Netherlands). Flow rates were calculated by the software from the product of measured velocity averaged over the lumen area multiplied by the cross-sectional area, in axially reformatted velocity images perpendicular to the tube, for each reconstructed phase. Flow volumes were calculated by integration over time. In addition, the maximal velocity was assessed. Contours were manually delineated on reconstructed velocity images by circular-shaped regions of interest with an enclosed area closely matching 0.79-cm$^2$ cross-sectional lumen area for the tube with 1.0-cm diameter and 0.38 cm$^2$ for the tube with 0.7-cm diameter. Relative flow-rate differences were calculated for each acquisition by comparison with timed volumetric collection, and relative differences in maximal velocity were calculated by comparison with 4DGRE, respectively.

For experiment 2, a pulsatile flow inside an LV phantom was created and imaged with MRI. This phantom consisted of a 0.5-mm-thick compliant silicone membrane that was manufactured by painting silicone onto a 3D-printed LV mold. The morphology was extracted from the statistical mean of segmented 4D CT images of 150 patients.[22,23] The LV phantom was filled with 60% glycerol/water solution. The setup is described in detail in Saaid et al.[24] The base of the membrane was connected to valve holders (Figure 2A) and immersed inside an acrylic tank. A pulsatile hydraulic piston pump (Vivitro Labs, Victoria, Canada) was connected to the tank with semirigid tubing. This pump, positioned outside the scanner room, generated a sinusoidal-like pulsatile waveform with 70-bpm frequency without net flow, resulting in a pressure waveform inside the tank that created contraction of the filled LV phantom with a 300-ms systolic period and 50-mL stroke volume. The outflow was directed through a one-way bioprosthetic aortic valve (AoV) and led back to the phantom through a bioprosthetic mitral valve (MV) (Figure 2A). The pump also generated a Transistor-Transistor-Logic trigger signal that was directly fed to a dedicated Transistor-Transistor-Logic input on the scanner for gating. The LV phantom was imaged by 4DEPI and 4DGRE using retrospective gating with 30 reconstructed phases over the pump cycle. The 4DEPI acquisition was performed in three different orthogonal orientations: 4DEPI5_ro_LA in long-axis orientation with the readout gradient parallel to the main inflow direction (i.e., along the long-axis from MV to apex), 4DEPI5_bp_LA with the blip phase-encoding gradient parallel to the main flow, and 4DEPI5_nbp_SA in short-axis orientation with the nonblip phase-encoding

gradient parallel to the main flow (Table 1, Figure 2B-D). The 4DGRE acquisition was performed only in long-axis orientation, identical to 4DEPI5_bp_LA. The scan time for 4DEPI was 3 minutes 37 seconds, and for 4DGRE it was 13 minutes 58 seconds.
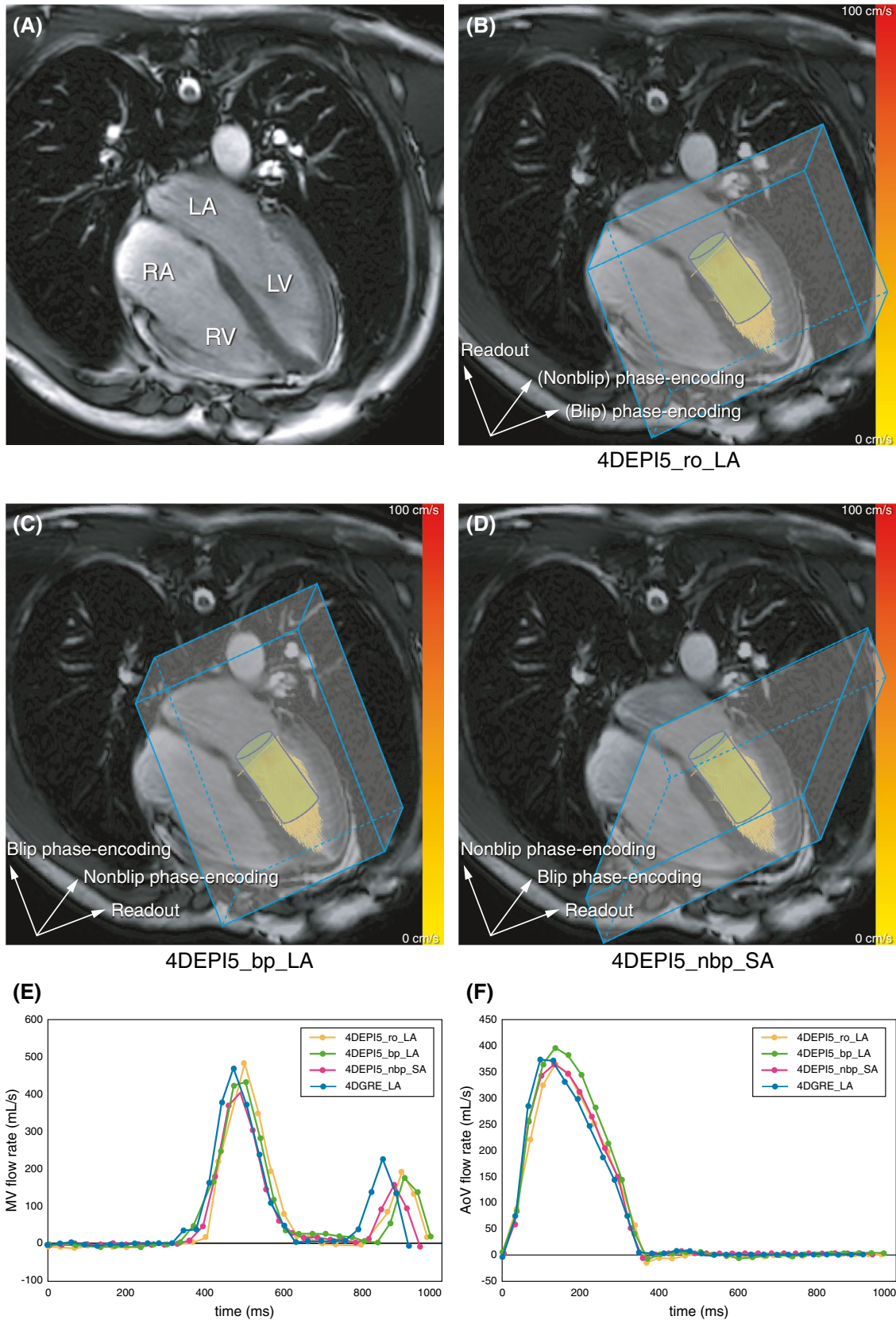
The 4DEPI and 4DGRE acquisitions were repeated without flow, after the pump was switched off (after >15 minutes of waiting, needed to annihilate all residual waves in the tank) and planned in the same orientation and scan order. The data of these acquisitions without flow were used for background phase offset correction by voxel-based velocity subtraction.[21] Speed comparison between respective acquisitions was performed using in-house-developed Python-based software. A cylindrical control volume (radius = 1.7 cm, length = 5.0 cm, containing 6401 measurement voxels) was manually positioned inside the LV phantom below the MV (Figure 2C), and its position was kept constant between scans. Voxel-based comparison of speed measured inside the control volume was performed by calculating differences between 4DGRE and the respective 4DEPI acquisitions for the time point of peak LV inflow. Moreover, for each of the 30 phases the median speed was calculated and compared between 4DGRE and 4DEPI. Voxel-based speed inside the LV is nonnormally distributed over space and time; therefore, spatial median and spatio-temporal median speed were calculated.

For experiment 3, 10 healthy volunteers (2 females and 8 males, mean age ± SD = 37 ± 12 years) were recruited. Informed consent was obtained. Data were collected as part of a sequence-optimization study that was approved
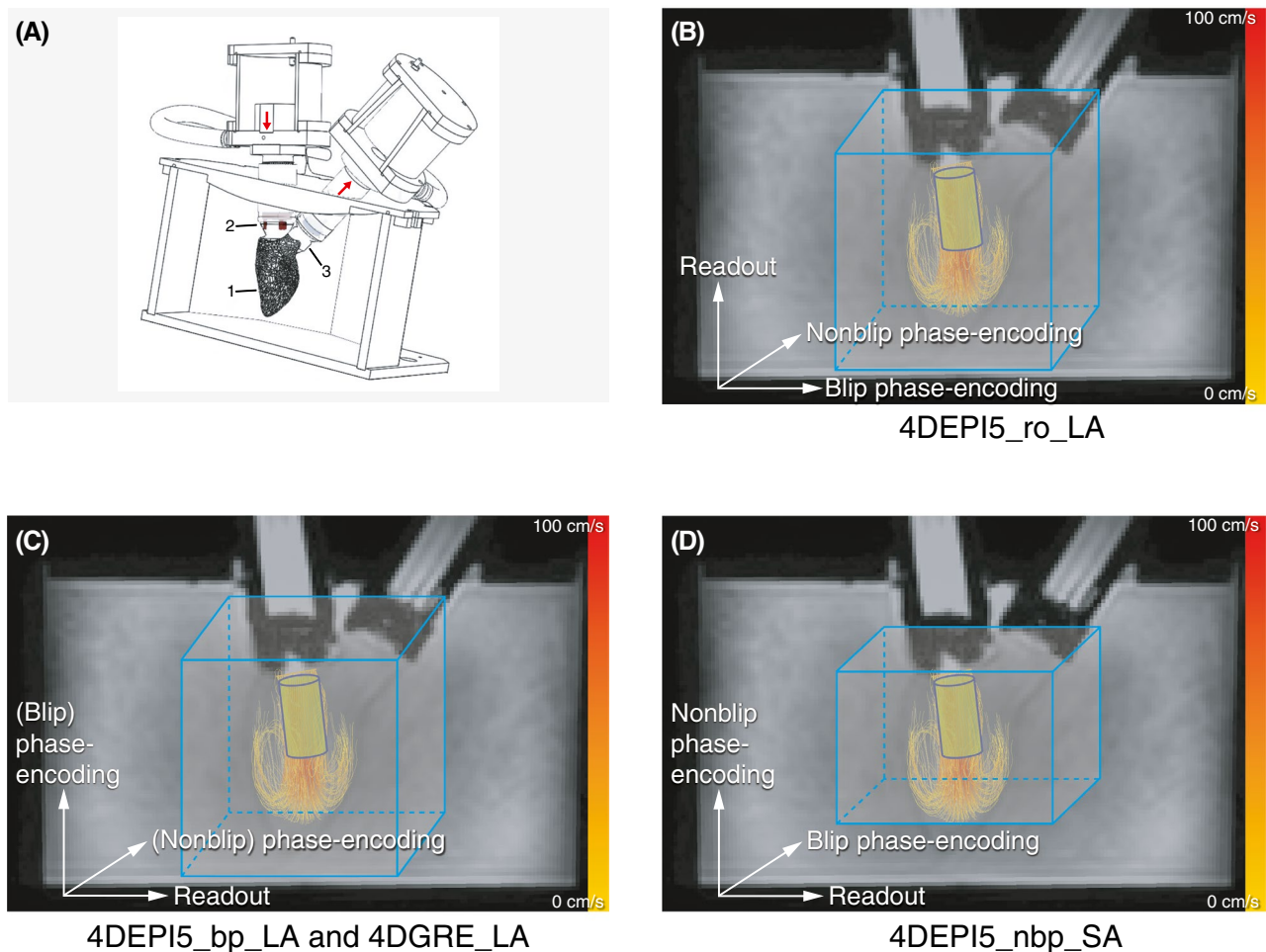


**FIGURE 2** Left-ventricle (LV) phantom setup in experiment 2. (A) Positioning of the pressurized acrylic tank in the scanner (1 indicates the LV phantom; 2 and 3 indicate the bioprosthetic mitral [MV] and aortic valve [AoV], respectively). (B–D) Illustrations of the gradient orientation for the three 4D-EPI (4DEPI) and 4DGRE acquisitions (4DEPI5_ro_LA refers to the long-axis-oriented EPI factor of 5 acquisition with the readout gradient aligned parallel to the main flow direction; 4DEPI5_bp_LA refers to the long-axis-oriented EPI acquisition with the blip phase-encoding gradient aligned parallel to the main flow direction; and 4DEPI5_nbp_SA refers to the short-axis-oriented EPI acquisition with the readout and blip phase-encoding gradient both perpendicular to the main flow direction). Color-coded streamlines are shown in the phantom during peak inflow. A blue cylinder-shaped control volume is positioned below the MV inside the ventricle. The schematically drawn scan volumes are not up to scale with the phantom dimensions

(A)

(B) 4DEPI5_ro_LA

(C) 4DEPI5_bp_LA

(D) 4DEPI5_nbp_SA

(E)

(F)

by the local Medical Ethical Committee. Each volunteer was scanned on the same 3T scanner as used for the phantom experiments. For each volunteer, one 4DGRE and three 4DEPI whole-heart 4D flow MRI acquisitions were

obtained. The 4DEPI acquisition was acquired first in long-axis orientation with the readout gradient aligned parallel to the main flow along the long-axis (4DEPI5_ro_LA), then in long-axis orientation with the blip phase-encoding

gradient parallel to the main flow (4DEPI5_bp_LA), and finally, in short-axis orientation with the nonblip phase-encoding gradient parallel to the main flow (4DEPI5_nbp_SA) (Table 1, Figure 3). The 4DGRE acquisition was acquired in the same orientation as 4DEPI5_ro_LA. The 4DEPI and 4DGRE acquisitions were repeated on a phantom filled with a static fluid, using the same positioning and orientation as for the respective volunteers, and in the same scanning order. Electrocardiogram triggering was simulated with simulated heart rates equal to the averaged heart rates measured for each healthy volunteer for the respective scans. These static phantom data were used for phase offset correction by voxel-based velocity subtraction.[21]

Before the 4D flow acquisitions, cine 2D left two-chamber and four-chamber views and coronal and sagittal views of the LV outflow tract were acquired using an SSFP sequence with TE/TR = 1.5/2.9 ms, FOV = 350 mm, 45° flip angle, and acquisition resolution = $2.0 \times 1.7 \times 8.0$ mm$^3$. These acquisitions were used for postprocessing (valve tracking) but also for scan planning. Retrospective gating was used with 30 phases reconstructed to represent one cardiac cycle. Sensitivity encoding with factor 2 was used. End-expiration breath holding was performed. Typical scan time for these acquisitions was 6 seconds for a 60-bpm heart rate.

The 4D flow data sets were visually inspected for artifacts. Valvular flow analysis was performed using *CAAS MR Solutions* 5.1 (Pie Medical Imaging, Maastricht, the Netherlands). First, the software performed anti-aliasing for each velocity direction and then phase offset correction by detecting static background signal. Then, automated retrospective valve tracking[25] of the MV and AoV was done using the left two-chamber and four-chamber cine SSFP series for the MV and the coronal and sagittal cine SSFP series of the LV outflow tract for the AoV. The MV and AoV net forward volumes (NFVs) were determined, as well as the difference between both. Next, median speed obtained from a control volume was compared between sequences, similar as in experiment 2. A cylindrical control volume was created with 1.2-cm radius and 2.5-cm length, containing on average $1693 \pm 25$ measurement voxels. This was visually positioned inside the LV below the MV (Figure 3). For each acquisition, the median

speed inside the control volume was determined for each cardiac phase, after voxel-based velocity subtraction using the static phantom data.

For the statistical analysis, the mean NFV ($\pm$ SD), averaged over the volunteers, was calculated per sequence as well as the relative differences and Pearson correlation r between AoV and MV NFV. Correlation was classified as poor (r < 0.50), moderate (r = 0.50–0.69), good (r = 0.70–0.84), very good (r = 0.85–0.94), and excellent (r ≥ 0.95). Differences in NFV between sequences were calculated and compared using paired t-tests and Bland-Altman analysis.[26] From the control volume inside the LV phantom, voxel-based speed comparison was performed for the time point of peak inflow. Mean differences (averaged over all voxels) and standard errors were calculated between sequences; paired t-tests were performed and Pearson correlation was calculated. Voxel-based speed inside the cardiac chambers is nonnormally distributed over space and time. Therefore, for each sequence, spatial median speed with interquartile range obtained from the control volume inside the LV phantom, as well as in the healthy volunteers, were calculated for each cardiac phase. Spatio-temporal median speed was calculated over the cardiac cycle. Because of nonnormality, comparison of median speed between sequences was done after logarithmic transformation to account for skewness of the distribution: For each sequence, logarithmic transformation of the median speed was performed first per cardiac phase. Median differences were calculated over the pump cycle or cardiac cycle, respectively, and back transformation resulted in ratios between median speed per sequence, as $^{10}$log (speed_4DEPI) $-$ $^{10}$log (speed_4DGRE) $=$ $^{10}$log (speed_4DEPI/speed_4DGRE). For the volunteers, mean ratios and SDs between sequences were compared using paired t-tests. A *p*-value < 0.05 was considered statistically significant. Analysis was performed using *SPSS* version 25 (IBM, Armonk, NY) with Python library NumPy version 1.15.0 and *Microsoft Excel for Mac* version 16.16.22.

## 3 | RESULTS

The results of experiment 1 are presented in Table 2. For experiments with 1-cm-diameter tube and 50-mL/s flow

**TABLE 2** Flow-rate assessment for steady flow in a straight tube (experiment 1)

| Acquisition | Volumetric flow rate (mL/s) | MRI-assessed flow rate (mL/s) | Relative difference (%) (ΔVolumetric) | MRI-assessed max velocity (cm/s) | Relative difference (%) (Δ4DGRE) | MRI-assessed flow rate (mL/s) | Relative difference (%) (ΔVolumetric) | MRI-assessed max velocity (cm/s) | Relative difference (%) (Δ4DGRE) |
|---|---|---|---|---|---|---|---|---|---|
| | | Tube 1 (diameter 1.0 cm) | | | | Tube 2 (diameter 0.7 cm) | | | |
| 4DEPI5_ro_coronal | 50 | 53.6 | 7.2 | 96 | 9.1 | 44.0 | −12.0 | 216 | −1.4 |
| 4DEPI5_bp_coronal | 50 | 53.0 | 6.1 | 97 | 10.2 | 45.0 | −10.0 | 216 | −1.4 |
| 4DEPI5_nbp_axial | 50 | 52.5 | 5.0 | 98 | 11.4 | 48.0 | −4.0 | 215 | −1.8 |
| 4DEPI3_ro_coronal | 50 | 54.0 | 8.0 | 88 | 0.0 | 49.1 | −1.8 | 233 | 6.4 |
| 4DEPI3_bp_coronal | 50 | 52.3 | 4.6 | 93 | 5.7 | 50.0 | 0 | 215 | −1.8 |
| 4DEPI3_nbp_axial | 50 | 51.6 | 3.1 | 92 | 4.5 | 46.7 | −6.6 | 229 | 4.6 |
| 4DGRE_coronal | 50 | 49.4 | −1.2 | 88 | – | 47.8 | −4.4 | 219 | – |
| 4DEPI5_ro_coronal | 23 | 24.3 | 5.7 | 44 | 2.3 | | | | |
| 4DEPI5_bp_coronal | 23 | 24.4 | 6.1 | 46 | 7.0 | | | | |
| 4DEPI5_nbp_axial | 23 | 23.9 | 3.9 | 42 | −2.3 | | | | |
| 4DGRE_coronal | 23 | 24.4 | 3.0 | 43 | – | | | | |

*Note*: 4DEPIx_ro refers to acquisition with EPI factor × (5 or 3) with the readout gradient aligned parallel to the main flow direction; 4DEPIx_bp refers to EPI acquisition with the blip phase-encoding gradient aligned parallel to the main flow direction; and 4DEPIx_nbp refers to EPI acquisition with the readout and blip phase-encoding gradient both perpendicular to the main flow direction.

rate, the largest measured relative difference in flow rate between 4DEPI5 with Venc of 120 cm/s and the timed volumetric collection is a 7.2% overestimation for 4DEPI5_ro_coronal, which is the acquisition with flow parallel to the readout gradient. The 4DGRE acquisition shows a small underestimation of 1.2%. Of note, the largest difference in maximal velocity when compared with 4DGRE is found for 4DEPI5_nbp_axial (11.4%) (i.e., flow perpendicular to the readout gradient and blip phase-encoding gradient). However, for the other two acquisitions, the difference in maximal velocity is approximately within the same order, close to 10%. For 4DEPI3, the difference in measured maximal velocity compared with 4DGRE decreases to below 6%, whereas the differences in flow rate compared with timed volumetric collection remains approximately within the same order, up to 8%.

For the 0.7-cm-diameter tube and therefore a higher flow velocity (imaged with Venc = 250 cm/s), the difference between 4DEPI and 4DGRE in measured maximal velocity is highest (6.4%) for 4DEPI3_ro_coronal, which is the acquisition with flow in the direction of the readout gradient. The difference in flow rate compared with timed volumetric collection is highest (12%) for 4DEPI5_ro_coronal, which is the acquisition also with flow in the direction of the readout gradient. Experiments with the 1-cm-diameter tube and low flow velocity (23 mL/s flow rate, imaged with Venc of 45 cm/s) show similar results as the experiments with 50-mL/s flow rate, although the differences in measured maximal velocity compared with 4DGRE are slightly smaller (largest difference is 7% for 4DEPI5_bp_coronal).

The results for experiment 2 obtained from the control volume inside the LV phantom are given in Table 3. Voxel-based speed comparison at peak inflow shows small (on average up to 2 cm/s) but statistically significant differences among the four acquisitions. Correlations between speed measurements from the respective acquisitions are very good to excellent (r ≥ 0.94, *p* < 0.01). In Supporting Information Figure S1, the distributions of speed measurements are presented for each acquisition for the time point of peak LV inflow and the next time point. From these histograms it is shown that speed is nonnormally distributed. Ratios of median speed comparing 4DEPI with 4DGRE show highest similarity (ratio = 0.981) for 4DEPI5_nbp_SA (i.e., with the main flow direction perpendicular to the readout and blip phase-encoding gradient). Differences in median speed between 4DEPI and 4DGRE for all orientations are within 5.5%.

For experiment 3, a total of 40 4D-flow MRI data sets were acquired in 10 healthy volunteers. Sample images of velocity data from 1 volunteer are shown in Supporting Information Figure S2. After visual inspection, one 4DEPI5_ro_LA data set was rejected for further evaluation due to unresolved

artifacts (most likely due to phase dispersion that could have been a result of subject movement during the acquisition) corrupting the velocity measurements (Figure 4). Automated retrospective MV and AoV tracking was performed, and forward and backward flow and NFV were assessed. The results are presented in Table 4 and Figure 5. Heart rates showed small but statistically significant differences between acquisitions: The average heart rate for 4DEPI5_ro_LA was significantly different from that of 4DEPI5_nbp_SA ($p = 0.04$) and 4DGRE_LA ($p = 0.04$). The mean relative NFV difference between MV and AoV (representing the amount of inconsistency in NFV between MV and AoV) was highest (6.4 ± 8.5%) for 4DEPI5_nbp_SA, but none of these differences were statistically significant. Very good to excellent correlations were found between MV and AoV NFV (r ≥ 0.89, $p < 0.01$), which is also illustrated in Figure 5. When comparing MV NFV and AoV NFV between acquisitions, some showed statistically significant differences: 4DEPI5_ro_LA was significantly different from 4DGRE_LA ($p = 0.01$); 4DEPI5_bp_LA was significantly different from 4DEPI5_nbp_SA ($p = 0.03$); and 4DEPI5_nbp_SA was significantly different from 4DGRE_LA ($p = 0.004$).

Values of median speed for the time point of peak early diastole obtained from the control volume are also provided in Table 4. The ratios of median speed comparing 4DEPI with 4DGRE over the full cycle are 0.91 or higher and show no statistically significant differences when compared between each other (4DEPI5_ro_LA/4DGRE_LA vs 4DEPI5_bp_LA/4DGRE_LA: $p = 0.40$; 4DEPI5_ro_LA/4DGRE_LA vs 4DEPI5_nbp_SA/4DGRE_LA: $p = 0.37$; and 4DEPI5_bp_LA/4DGRE_LA vs 4DEPI5_nbp_SA/4DGRE_LA: $p = 0.77$).

## 4 | DISCUSSION

In this study, we evaluated how the use of 4DEPI with moderate EPI factor 5 negatively affects velocity and flow rate in in vitro experiments and in vivo whole-heart 4D flow MRI. The main finding is the confirmation that for in vivo and in vitro 4DEPI, flow in the direction of the EPI readout or blip phase-encoding gradient results in statistically significant differences in velocity and flow rate (when compared with 4DGRE), as was also described by Dillinger et al based on in silico and in vitro experiments.[18] However, mean differences in flow rate, voxel-based speed, and spatio-temporal median speed averaged over 10 healthy volunteers were acceptable (≤10%) when comparing 4DEPI (with EPI factor 5) and 4DGRE for normal in vivo intracardiac flow. The error in flow rate was smallest (<2%) when readout and blip phase-encoding gradient were both perpendicular to the main flow direction.

Dillinger et al[18] performed in silico simulations of 4DEPI with EPI factor 5 and 4DGRE with steady flow. They showed errors larger than 40% for local (peak) velocities distal to a stenosis that was located proximal to a U-bend phantom, at high-flow conditions of 2.2 m/s for 4DEPI with the readout gradient parallel to the flow direction. Their setup may not be directly comparable to our experiment 1. In a straight tube with maximal flow velocity near 2.2 m/s, we found the highest error in flow rate to be 12%, when flow was parallel to the readout gradient. Although such high-flow conditions are not usually present in normal intracardiac flow or in patients with up to moderate valvular diseases, 4DEPI may not be the appropriate acceleration technique for

**TABLE 3** Voxel-based comparison of speed sampled inside the control volume at peak inflow in the LV phantom and comparison of median speed and interquartile range (in centimeters/second) (experiment 2)

| Voxel-based comparison at peak LV inflow | Mean difference ± SEM (cm/s) | $p$-Value t-test | Pearson correlation ($p$-value) |
|---|---|---|---|
| 4DEPI5_ro_LA–4DGRE_LA | −1.28 ± 0.12 | << 0.01 | 0.94 ($p < 0.01$) |
| 4DEPI5_bp_LA–4DGRE_LA | −2.16 ± 0.09 | << 0.01 | 0.97 ($p < 0.01$) |
| 4DEPI5_nbp_SA–4DGRE_LA | −1.01 ± 0.11 | << 0.01 | 0.95 ($p < 0.01$) |
| 4DEPI5_ro_LA–4DEPI5_bp_LA | 0.87 ± 0.12 | << 0.01 | 0.94 ($p < 0.01$) |
| 4DEPI5_ro_LA–4DEPI5_nbp_SA | −0.27 ± 0.08 | << 0.01 | 0.97 ($p < 0.01$) |
| 4DEPI5_bp_LA–4DEPI5_nbp_SA | −1.14 ± 0.12 | << 0.01 | 0.94 ($p < 0.01$) |
| **Median speed (over all time points)** | **Median (IQR) (cm/s)** | **4DEPI/4DGRE ratio (over all time points)** | |
| 4DEPI5_ro_LA | 24.2 (15.6, 39.7) | 0.945 | |
| 4DEPI5_bp_LA | 24.2 (15.6, 40.6) | 0.954 | |
| 4DEPI5_nbp_SA | 24.8 (15.6, 42.9) | 0.981 | |
| 4DGRE_LA | 25.4 (15.7, 42.1) | | |

*Note:* 4DEPI5_ro_LA refers to EPI factor of 5 acquisition with the readout gradient aligned parallel to the main flow direction; 4DEPI5_bp_LA refers to EPI acquisition with the blip phase-encoding gradient aligned parallel to the main flow direction; and 4DEPI5_nbp_SA refers to EPI acquisition with the readout and blip phase-encoding gradient both perpendicular to the main flow direction. Abbreviation: IQR, interquartile range.
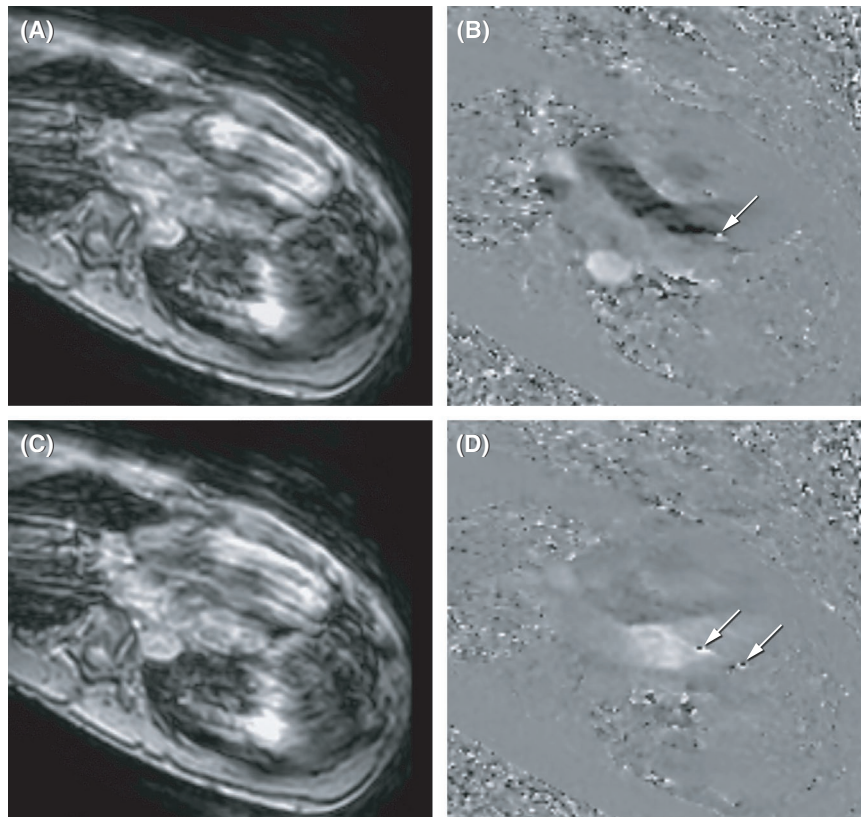
**FIGURE 4** Artifacts present in velocity images of one 4DEPI5_ro_LA data set in a healthy volunteer (arrows in [B] and [D]). (A,B) Systolic phase. (C,D) Diastolic phase. Artifacts appear with phase wrapping but in areas with moderate velocities, and therefore remain unresolved by anti-aliasing algorithm. This particular data set was removed from analysis

**TABLE 4** Valvular flow assessment by automated retrospective valve tracking over the MV and AoV and median speed assessed from the control volume in the LV of 10 healthy volunteers (experiment 3)

| | 4DEPI5_ro_LA | 4DEPI5_bp_LA | 4DEPI5_nbp_SA | 4DGRE_LA |
|---|---|---|---|---|
| Mean heart rate ± SD (bpm) | 57 ± 7 | 59 ± 7 | 60 ± 6 | 60 ± 4 |
| Mean MV FF ± SD (mL/beat) | 92 ± 26 | 100 ± 23 | 93 ± 21 | 103 ± 17 |
| Mean MV BF ± SD (mL/beat) | 2 ± 2 | 4 ± 4 | 2 ± 1 | 4 ± 3 |
| Mean MV NFV ± SD (mL/beat) | 90 ± 24 | 95 ± 22 | 92 ± 20 | 99 ± 16 |
| Mean AoV FF ± SD (mL/beat) | 93 ± 22 | 99 ± 21 | 98 ± 18 | 99 ± 18 |
| Mean AoV BF ± SD (mL/beat) | 1 ± 1 | 1 ± 1 | 1 ± 1 | 2 ± 2 |
| Mean AoV NFV ± SD (mL/beat) | 93 ± 21 | 96 ± 20 | 97 ± 17 | 96 ± 17 |
| Mean relative difference (AoV NFV − MV NFV) ± SD (%) | 4.2 ± 6.8 | 1.6 ± 6.0 | 6.4 ± 8.5 | −2.9 ± 7.4 |
| t-test (AoV NFV vs MV NFV) | 0.16 | 0.60 | 0.08 | 0.28 |
| Pearson r (AoV NFV vs MV NFV) | 0.97 ($p < 0.01$) | 0.97 ($p < 0.01$) | 0.89 ($p < 0.01$) | 0.91 ($p < 0.01$) |
| Median speed at peak diastole (IQR) (cm/s) | 51.4 (41.5, 63.8) | 46.7 (44.8, 61.7) | 56.6 (45.8, 59.4) | 51.6 (45.2, 68.6) |
| Mean EPI/GRE ratio ± SD (over all cardiac phases) | 0.91 ± 0.08 | 0.94 ± 0.10 | 0.93 ± 0.06 | |

*Note:* 4DEPI5_ro_LA refers to EPI factor of 5 acquisition with the readout gradient aligned parallel to the main flow direction; 4DEPI5_bp_LA refers to EPI acquisition with the blip phase-encoding gradient aligned parallel to the main flow direction; and 4DEPI5_nbp_SA refers to EPI acquisition with the readout and blip phase-encoding gradient both perpendicular to the main flow direction.

Abbreviations: BF, backward flow; FF, forward flow; NFV, net forward volume.

measuring peak velocity, especially in a stenotic or regurgitant jet with high velocity parallel to the readout or blip phase-encoding gradient. Furthermore, 4DEPI may not be advised for evaluation of complex vasculatures such as in the brain, when flow changes in direction or the main flow direction is unknown. Even for the aortic arch, high flow velocity along the readout or blip phase-encoding gradient cannot be avoided, as was evident from simulations described by Dillinger et al in the U-bend phantom. However, the performance of 4DEPI
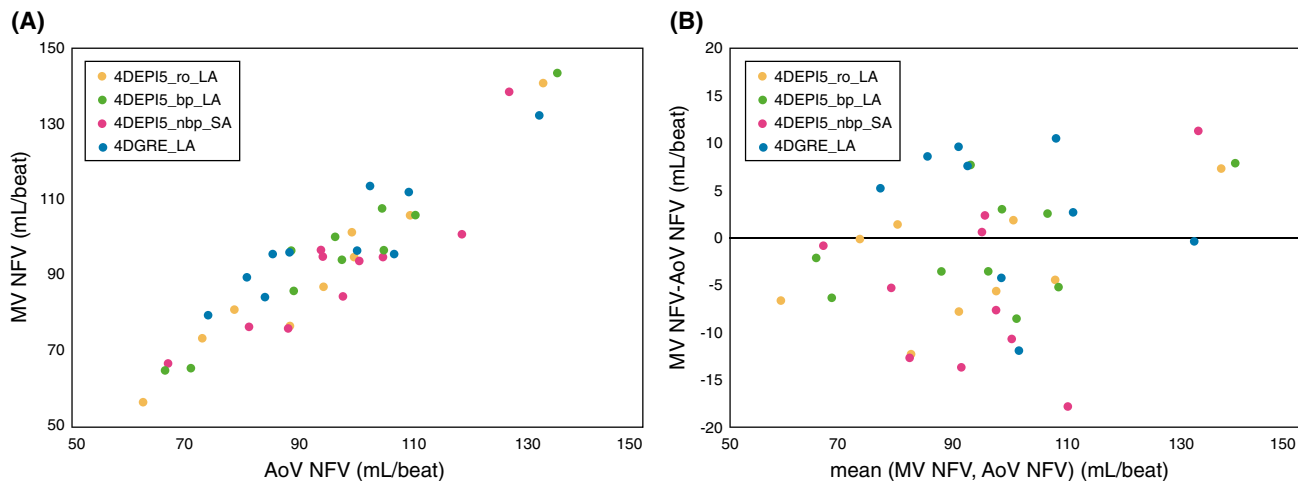
**FIGURE 5** Net forward volume (NFV) measured over MV and AoV assessed in 10 healthy volunteers by four acquisitions. Bland-Altman plot is presented in (B)

with both the readout and blip phase-encoding gradient perpendicular to the main flow direction was not part of their experiments. For that orientation, velocity data are not compromised by velocity-dependent phase shifts in readout gradient direction, nor by a modulated point spread function by accumulated phase shifts in the blip phase-encoding gradient direction. Therefore, differences in speed or flow rate for 4DEPI in this scan orientation compared with 4DGRE are, as expected, indeed smaller. Because EPI acquisition requires a longer TE for this orientation, the flow displacement still negatively affects accuracy.

Our steady-flow experiment (experiment 2) showed that for flow velocity in normal intracardiac range (<1 m/s) and EPI factor 5, the highest error (7.2%) in flow rate was found for 4DEPI with flow parallel to the readout gradient and lowest (5.0%) when oriented with flow perpendicular to the readout and blip phase-encoding gradient. This is in line with the results from a previously published study of a pulsatile phantom scanned with 4DEPI.[12] Furthermore, in experiment 2 we evaluated the choice of EPI factor on the accuracy of flow rate and velocity. We did not find a substantial improvement nor systematic trend in accuracy when lowering the EPI factor from 5 to 3, but with the software release used on our scanner, we could not evaluate higher EPI factors. Additionally, for slow flow imaged with a Venc of 45 cm/s, also no systematic trend in accuracy was found. Of note, because 4DGRE is not affected by gradient orientation–related sources of error in the same way as 4DEPI, only one single 4DGRE scan orientation was acquired in our experiments.

In experiment 2, voxel-based speed comparison was performed. Differences in speed among the 4DEPI acquisitions compared with 4DGRE and compared among each orientation were statistically significant but small

(on average up to 2 cm/s). Comparison of median speed between 4DEPI with 4DGRE showed highest similarity when readout and blip phase-encoding gradient were perpendicular to the main flow direction, which is in line with the results of experiment 1.

In experiment 3, 4DEPI was compared with 4DGRE in 10 healthy volunteers. Valvular flow assessment showed statistically significant differences between 4DEPI5 and 4DGRE, but the differences are smaller than 5% and may be considered clinically nonsignificant. Surprisingly, and in contrast to the results of experiments 1 and 2, the inconsistency in NFV quantitation at MV and AoV was highest for 4DEPI5_nbp_SA, with readout and blip phase-encoding gradient perpendicular to the LV inflow direction; however, the differences were not statistically significant. Also, it must be noted that interscan variation cannot be ruled out. The acquisition time was much longer for 4DGRE (ranging between 19 minutes 49 seconds and 25 minutes 9 seconds) than for 4DEPI (ranging between 5 minutes 18 seconds and 6 minutes 40 seconds). Therefore, 4DGRE may be more exposed to subject's motion, heart-rate variability, and changes in breathing pattern. The measured heart rates were slightly but statistically significantly different between the acquisitions, which may be an indicator for interscan variation. Still, the reported inconsistencies in NFV are small and acceptable for all 4DEPI and 4DGRE acquisitions when compared with the previously reported scan–rescan variability of 12% in valvular flow assessment.[27]

For the reference 4DGRE acquisition, nonsegmented k-space GRE was used, resulting in relatively long scan times. Segmented k-space GRE is significantly faster, making the difference in scan time with 4DEPI smaller. For this study, non-EPI accelerated 4DGRE was compared with 4DEPI to single out the effects of EPI readout on the

quantitation of flow volume and velocity, similarly to the approach of Dillinger et al.[18] Additionally, conventional SENSE with a moderate acceleration factor 2 was applied (both for 4DEPI and 4DGRE). Other acceleration techniques, such as compressed sensing,[28,29] were not compared with 4DEPI in this study.

For in vivo LV flow, spatio-temporal median speed was consistently higher for 4DGRE than for 4DEPI, with a largest mean difference of 9% when the readout gradient was parallel to the main flow direction. Of note, flow displacement is expected to be larger for all 4DEPI sequences due to prolonged TEs compared with 4DGRE. In the case of the highest measured median speed at peak diastole (56.6 cm/s measured for 4DEPI5_nbp_SA), flow displacement may be as large as 2.8 mm for 4DEPI (vs 1.4 mm for 4DGRE), which approximates the acquisition voxel dimension and therefore may not be neglected.

Dillinger et al[18] compared local peak velocities between MRI and computational fluid dynamics. In experiment 2 of the current study, voxel-based speed comparison was performed between acquisitions for all voxels inside a control volume that was positioned below the MV and at the time point of peak LV inflow. In vivo, we compared 4D velocity fields by calculating spatial median and spatio-temporal median speed. The median was used, as LV velocities are nonnormally distributed over time and space. Median speed itself may not have clinical relevance but is used here as a statistical representative measure of a velocity field in the evaluation of differences between acquisitions. Direct voxel-based comparison is not feasible in vivo due to potential misregistration between the respective 4D velocity fields. Moreover, velocities measured at one specific point in space and time are subjected to noise and other sources of error such as artifacts, heart-rate variability, or misregistration. Still, it needs to be noted that the error in local speed at a single voxel and a single time point may be much higher than the error in median speed. Of note, in addition in vivo comparison of median speed, in this study we compared MV and AoV forward and backward flow volumes, NFV, and inconsistency in NFV between valves, all parameters that are of immediate clinical interest.

Our study has some limitations. Only 4DEPI with EPI with factors 3 and 5 were evaluated. Higher EPI factors were not allowed for 4D flow with the software release used on our MRI system. Although not evident from our results comparing 4DEPI5 versus 4DEPI3, it is expected that using higher EPI factors would lead to higher inaccuracies due to more phase accumulation, more severe modulation of the point spread function, and more severe flow displacement. Various clinical studies have shown

that EPI factor 5 can provide acceleration with acceptable scanning time in combination with acceptable accuracy, especially when the acquisition volume can be planned with readout and blip phase-encoding gradient both perpendicular to the main flow direction.[12,13,30–34]

The receiver bandwidth was substantially different between the respective 4DEPI and 4DGRE acquisitions. In this study, acquisition parameters were kept identical between 4DGRE and 4DEPI, which resulted in bandwidth differences. In theory, the bandwidth could be manually reduced by adjusting the water–fat shift, but for 4DEPI this would imply a longer echo spacing, which would make 4DEPI even more sensitive to flow artifacts.

No respiratory control has been used during 4D flow acquisitions, neither for 4DEPI nor for 4DGRE. It has been shown that 4D flow MRI without respiratory gating can be acquired with preserved data quality when compared to acquisition with respiratory gating.[35,36] Furthermore, we expect respiration motion blurring to have a similar effect on 4DEPI as well as 4DGRE.

Finally, in vivo intracardiac flow was only tested in healthy volunteers. Ethical considerations hindered an extensive clinical evaluation with repeated 4DEPI acquisitions in various orientations and a long 4DGRE acquisition in patients. Nevertheless, implementations of 4DEPI in volunteers and patients with various cardiac diseases with up to moderate valve regurgitation have proven to be of clinical value.[12,13,25,28–34]

## 5 | CONCLUSIONS

When flow is present in the direction of the EPI readout or blip phase-encoding gradient, EPI acceleration on 4D flow MRI results in less accurate velocity and flow rate than for non-EPI accelerated 4D flow MRI. However, mean differences in flow rate, voxel-based speed, and spatio-temporal median speed when comparing 4DEPI and 4DGRE over 10 healthy volunteers were acceptable (≤10%) for normal intracardiac flow with EPI factor 5. Transvalvular forward flow volumes over mitral or aortic valve are on average less than 6.4% different when acquired with 4DEPI compared to 4DGRE. Standard 4DGRE remains the most accurate acquisition for intracardiac 4D flow MRI. When using 4DEPI, to minimize errors in velocity and flow rate, it is recommended to plan the acquisition such that readout and blip phase-encoding gradient are both perpendicular to the anticipated main flow direction.

## CONFLICT OF INTEREST

## DATA AVAILABILITY STATEMENT

Data can be made available upon reasonable request.

## ORCID

Jos J. M. Westenberg ⓘ https://orcid.org/0000-0003-1946-1715

## REFERENCES

1. Wigström L, Sjöqvist L, Wranne B. Temporally resolved 3D phase-contrast imaging. *Magn Reson Med*. 1996;36:800-803.
2. Bogren HG, Buonocore MH. 4D magnetic resonance velocity mapping of blood flow patterns in the aorta in young vs. elderly normal subjects. *J Magn Reson Imaging*. 1999;10:861-869.
3. Wigström L, Ebbers T, Fyrenius A, et al. Particle trace visualization of intracardiac flow using time-resolved 3D phase contrast MRI. *Magn Reson Med*. 1999;41:793-799.
4. Pruessmann KP, Weiger M, Scheidegger MB, Boesiger P. SENSE: sensitivity encoding for fast MRI. *Magn Reson Med*. 1999;42:952-962.
5. Beerbaum P, Korperich H, Gieseke J, Barth P, Peuster M, Meyer H. Rapid left-to-right shunt quantification in children by phase-contrast magnetic resonance imaging combined with sensitivity encoding (SENSE). *Circulation*. 2003;108:1355-1361.
6. Thunberg P, Karlsson M, Wigstrom L. Accuracy and reproducibility in phase contrast imaging using SENSE. *Magn Reson Med*. 2003;50:1061-1068.
7. Beerbaum P, Korperich H, Gieseke J, Barth P, Peuster M, Meyer H. Blood flow quantification in adults by phase-contrast MRI combined with SENSE—a validation study. *J Cardiovasc Magn Reson*. 2005;7:361-369.
8. Uribe S, Beerbaum P, Sørensen TS, Rasmusson A, Razavi R, Schaeffter T. Four-dimensional (4D) flow of the whole heart and great vessels using real-time respiratory self-gating. *Magn Reson Med*. 2009;62:984-992.
9. Stadlbauer A, van der Riet W, Crelier G, Salomonowitz E. Accelerated time-resolved three-dimensional MR velocity mapping of blood flow patterns in the aorta using SENSE and k-t BLAST. *Eur J Radiol*. 2010;75:e15-e21.
10. DeLaPaz RL. Echo-planar imaging. *Radiographics*. 1994;14:1045-1058.
11. Kozerke S, Hasenkam JM, Pedersen EM, Boesiger P. Visualization of flow patterns distal to aortic valve prostheses in humans using a fast approach for cine 3D velocity mapping. *J Magn Reson Imaging*. 2001;13:690-698.
12. Westenberg JJM, Roes SD, Ajmone Marsan N, et al. Mitral valve and tricuspid valve blood flow: accurate quantification with 3D velocity-encoded MR imaging with retrospective valve tracking. *Radiology*. 2008;249:792-800.
13. Roes SD, Hammer S, van der Geest RJ, et al. Flow assessment through four heart valves simultaneously using 3-dimensional 3-directional velocity-encoded magnetic resonance imaging with retrospective valve tracking in healthy volunteers and patients with valvular regurgitation. *Invest Radiol*. 2009;44:669-675.
14. Duerk JL, Simonetti OP. Theoretical aspects of motion sensitivity and compensation in echo-planar imaging. *J Magn Reson Imaging*. 1991;1:643-650.
15. Butts K, Riederer SJ. Analysis of flow effects in echo-planar imaging. *J Magn Reson Imaging*. 1992;2:285-293.
16. Nishimura DG, Irarrazabal P, Meyer CH. A velocity k-space analysis of flow effects in echo-planar and spiral imaging. *Magn Reson Med*. 1995;33:549-556.
17. Nishimura DG, Jackson JI, Pauly JM. On the nature and reduction of the displacement artifact in flow images. *Magn Reson Med*. 1991;22:481-492.
18. Dillinger H, Walheim J, Kozerke S. On the limitations of echo planar 4D flow MRI. *Magn Reson Med*. 2020;84:1806-1816.
19. Pelc NJ, Bernstein MA, Shimakawa A, Glover GH. Encoding strategies for three-direction phase-contrast MR imaging of flow. *J Magn Reson Imaging*. 1991;1:405-413.
20. Westenberg JJM, Wasser MNJM, van der Geest RJ, et al. Scan optimization of gadolinium contrast-enhanced three-dimensional MRA of peripheral arteries with multiple bolus injections and in vitro validation of stenosis quantification. *Magn Reson Imaging*. 1999;17:47-57.
21. Hofman MBM, Rodenburg MJA, Markenroth Bloch K, et al. In-vivo validation of interpolation-based phase offset correction in cardiovascular magnetic resonance flow quantification: a multi-vendor, multi-center study. *J Cardiovasc Magn Reson*. 2019;21:30.
22. Metz CT, Baka N, Kirisli H, et al. Regression-based cardiac motion prediction from single-phase CTA. *IEEE Trans Med Imaging*. 2012;31:1311-1325.
23. Kirişli HA, Schaap M, Klein S, et al. Evaluation of a multi-atlas based method for segmentation of cardiac CTA data: a large-scale, multicenter, and multivendor study. *Med Phys*. 2010;37:6279-6291.
24. Saaid H, Voorneveld J, Schinkel C, et al. Tomographic PIV in a model of the left ventricle: 3D flow past biological and mechanical heart valves. *J Biomech*. 2019;90:40-49.
25. Kamphuis VP, Roest AAW, Ajmone Marsan N, et al. Automated cardiac valve tracking for flow quantification with four-dimensional flow MRI. *Radiology*. 2019;290:70-78.
26. Bland JM, Altman DG. Statistical methods for assessing agreement between two methods of clinical measurement. *Lancet*. 1986;1:307-310.
27. Kamphuis VP, van der Palen RLF, de Koning PJH, et al. In-scan and scan–rescan assessment of LV in- and outflow volumes by 4D flow MRI versus 2D planimetry. *J Magn Reson Imaging*. 2018;47:511-522.
28. Walheim J, Dillinger H, Kozerke S. Multipoint 5D flow cardiovascular magnetic resonance—accelerated cardiac- and respiratory-motion resolved mapping of mean and turbulent velocities. *J Cardiovasc Magn Reson*. 2019;21:42.
29. Ma LE, Markl M, Chow K, et al. Aortic 4D flow MRI in 2 minutes using compressed sensing, respiratory controlled adaptive k-space reordering, and inline reconstruction. *Magn Reson Med*. 2019;81:3675-3690.
30. Marsan NA, Westenberg JJM, Ypenburg C, et al. Quantification of functional mitral regurgitation by real-time 3D echocardiography: comparison with 3D velocity-encoded cardiac magnetic resonance. *JACC Cardiovasc Imaging*. 2009;2:1245-1252.
31. Marsan NA, Westenberg JJM, Roes SD, et al. Three-dimensional echocardiography for the preoperative assessment of patients with left ventricular aneurysm. *Ann Thorac Surg*. 2011;91:113-121.

32. Ewe SH, Delgado V, van der Geest R, et al. Accuracy of three-dimensional versus two-dimensional echocardiography for quantification of aortic regurgitation and validation by three-dimensional three-directional velocity-encoded magnetic resonance imaging. *Am J Cardiol*. 2013;112:560-566.

33. Driessen MMP, Schings MA, Sieswerda GT, et al. Tricuspid flow and regurgitation in congenital heart disease and pulmonary hypertension: comparison of 4D flow cardiovascular magnetic resonance and echocardiography. *J Cardiovasc Magn Reson*. 2018;20:5.

34. van Wijk WHS, Breur JMPJ, Westenberg JJM, et al. Validation of aortic valve 4D flow analysis and myocardial deformation by cardiovascular magnetic resonance in patients after the arterial switch operation. *J Cardiovasc Magn Reson*. 2019;21:20.

35. Kanski M, Töger J, Steding-Ehrenborg K, et al. Whole-heart four-dimensional flow can be acquired with preserved quality without respiratory gating, facilitating clinical use: a head-to-head comparison. *BMC Med Imaging*. 2015;15:20.

36. Nordmeyer S, Riesenkampff E, Crelier G, et al. Flow-sensitive four-dimensional cine magnetic resonance imaging for offline blood flow quantification in multiple vessels: a validation study. *J Magn Reson Imaging*. 2010;32:677-683.

## SUPPORTING INFORMATION

Additional supporting information may be found in the online version of the article at the publisher's website.

**FIGURE S1** Histograms of velocity magnitude (i.e., speed) distribution, measured in centimeters per second from the 6401 voxels inside the control volume in the left-ventricular (LV) phantom for the four respective acquisitions. A, Distribution at the time point of peak LV inflow. B, The next consecutive time point

**FIGURE S2** Example magnitude and phase images at the time point of peak early diastole of the three 4D-EPI (4DEPI) sequences and 4D gradient-echo (4DGRE) in the same volunteer. Phase image represents the main flow direction

**TABLE S1A** Magnetic resonance imaging acquisition details from experiment 1

**TABLE S1B** Magnetic resonance imaging acquisition details from experiments 2 and 3